minerals

MDPI

Article

Mineralogical Associations of Sedimentary Arsenic within a Contaminated Aquifer Determined through Thermal Treatment and Spectroscopy

Thomas S. Varner [1,*], Harshad V. Kulkarni [1,2], Mesbah Uddin Bhuiyan [3], M. Bayani Cardenas [4], Peter S. K. Knappett [5] and Saugata Datta [1,*]

1 Department of Earth and Planetary Sciences, University of Texas at San Antonio, San Antonio, TX 78249, USA; harshad@iitmandi.ac.in
2 School of Civil and Environmental Engineering, Indian Institute of Technology Mandi, Mandi 175005, Himachal Pradesh, India
3 Department of Oceanography, Noakhali Science and Technology University, Noakhali 3814, Bangladesh
4 Department of Geological Sciences, The University of Texas at Austin, Austin, TX 78712, USA
5 Department of Geology and Geophysics, Texas A&M University, College Station, TX 77843, USA
* Correspondence: tom.varner@my.utsa.edu (T.S.V.); saugata.datta@utsa.edu (S.D.)

Abstract: Sedimentary arsenic (As) in the shallow aquifers of Bangladesh is enriched in finer-grained deposits that are rich in organic matter (OM), clays, and iron (Fe)-oxides. In Bangladesh, sediment color is a useful indicator of pore water As concentrations. The pore waters of orange sediments are usually associated with lower As concentrations (<50 µg/L) owing to abundant Fe-oxides which sorb As. Using this color signal as a guide, spectroscopic measurements alongside thermal treatment were extensively utilized for analyzing the properties of both Fe-oxides and clay minerals. This study uses Fourier transform infrared (FTIR) and diffuse reflectance (DR) measurements along with thermal treatment to evaluate the solid-phase associations of As from sediment collected along the Meghna River in Bangladesh. The samples analyzed in this study were chosen to represent the various lithologies present at the study site and included riverbank sands (1 m depth), silt (6 m depth), aquifer sand (23 m depth), and a clay aquitard (37 m depth). The concentrations of sedimentary As and Fe were measured by X-ray fluorescence, and the spectroscopic measurements were taken on the samples prior to the thermal treatment. For the thermal treatment, sediment samples were placed in a preheated furnace at 600 °C for 3 h. The thermal treatment caused a deepening of reddish-brown hues in all samples, and the greatest change in color was observed in the finer-grained samples. The FTIR spectral analysis revealed that the clay minerals were composed primarily of illite, smectite, and kaolinite. The DR results indicate that the majority of Fe in sands was present as goethite; however, in the clay and silt samples, Fe was incorporated into the structure of clay minerals as Fe(II). The amount of structural Fe(II) was strongly positively correlated with the sedimentary As concentrations, which were highest in the finer-grained samples. After thermal treatment, the concentrations of As in the finer-grained samples decreased by an average of 40%, whereas the change in the As concentrations of the sand samples was negligible. These findings indicate that significant proportions of solid-phase As may be retained by OM and Fe(II)-bearing clay minerals.

Keywords: arsenic; diffuse reflectance; iron-oxide; Meghna River; clay mineral; colorimetry; Bangladesh

Citation: Varner, T.S.; Kulkarni, H.V.; Bhuiyan, M.U.; Cardenas, M.B.; Knappett, P.S.K.; Datta, S. Mineralogical Associations of Sedimentary Arsenic within a Contaminated Aquifer Determined through Thermal Treatment and Spectroscopy. *Minerals* **2023**, *13*, 889. https://doi.org/10.3390/min13070889

Academic Editors: Maria Economou-Eliopoulos and Pierfranco Lattanzi

Received: 26 March 2023
Revised: 16 June 2023
Accepted: 21 June 2023
Published: 30 June 2023

1. Introduction

Dissolved geogenic arsenic (As) pollution in the shallow aquifers (<60 m) of the Bengal basin threatens the health of millions who rely on the groundwater as their primary source of drinking water [1–3]. Recent deposition of As-bearing sediments throughout the Holocene from the weathering of As-rich parent rocks along the Himalayan orogenic belt was implicated as the primary source of dissolved As in the shallow aquifers of the

Bengal basin [4–6]. However, the regional occurrence of geogenic As in the Bengal basin and the heterogeneous distribution of dissolved As concentrations within the Holocene aquifers complicated efforts to determine the exact nature of As in the sediments that is easily mobilized and dissolved into the groundwater.

The release of As from iron (Fe) minerals is primarily attributed to the microbial-mediated dissolution of Fe-oxide coatings on sand grains and clay minerals, fueled by labile organic matter [7–17]. While the reductive dissolution of Fe-oxides can explain a significant proportion of the As released to solution, it is worth noting that secondary minerals, including Fe-oxides, are diagenetically formed within the sediment. Consequently, several other constituents, such as micaceous minerals, clays [14,18–20], and organic matter [21,22], were identified as hosts for As in the solid phase within the aquifer sediment. Although the behavior of Fe-oxide minerals plays a prominent role in the sequestration and mobilization of the dissolved As, the precise nature of the association between solid-phase As and other Fe and clay mineral hosts, as well as their mobilizing pathways within the aquifer, remains uncertain.

Despite the consistently higher presence of As in organic-rich silt and clay sediments in the Bengal basin [4,11,23–26], relatively few studies focused on the effects of clay/phyllosilicate minerals on the solid-phase partitioning of As in the shallow aquifers of Bangladesh. These finer-grained sediments often contain abundant organic matter (OM) with an affinity for strongly adsorbing As [21,22,27–29]. Additionally, these finer-grained sediments consist of clay/phyllosilicate minerals capable of adsorbing or incorporating As in the mineral structure [19,20,30–34]. Furthermore, reduced Fe(II) in the structure of clay minerals is highly reactive with the environment [35–38], and allows for the effective trapping of As and OM [39]. The presence of these Fe-bearing clay minerals, which account for over 50% of the Fe mass in subsurface soils [40–42], may contribute to the enrichment of solid-phase As in the finer-grained sediments. Despite numerous observations regarding the co-occurrence of As with Fe, OM, and clay minerals, there is still limited understanding of the extent to which these clay minerals influence the availability and mobility of As in the Bengal basin.

The use of Fourier transform infrared spectroscopy (FTIR) is remarkably well suited for the detection of hydroxyl units and oxygen bonds in samples; it was therefore extensively used for the identification of clay minerals as well as Fe-oxides and Fe-oxy(hydroxides) [43–49]. Additionally, due to the variety of hues exhibited by Fe-oxides, diffuse reflectance (DR) is a useful tool for the simple differentiation of individual Fe-oxide species present that reflect and absorb differently in the red and blue spectral regions [50]. The combined use of FTIR and DR techniques provides a powerful framework for the identification of the most prominent Fe-oxide and clay minerals present in a bulk sediment sample.

The effects of temperature on the mineralogy of clays and Fe-oxides are well documented because an understanding of the impacts on the composition of these minerals from elevated temperatures is crucial for the optimal production of pigments, dyes, ceramics, and bricks [51–54]. For example, the dehydroxylation of amorphous Fe and goethite begins at temperatures around 200 °C and transformation into hematite occurs above 300 °C, whereas phyllosilicate minerals experience dehydration, oxidation, dehydroxylation, and decomposition as temperatures increase from 100 °C to ~1000 °C, although the range differs for various minerals [55,56]. Given the unique responses of various oxides, clay minerals, and OM to high temperatures, such thermal treatment can induce changes in the sediment to allow for the rapid identification of the prominent constituents.

While the utilization of FTIR and DR for analyzing thermally treated clays and ceramics is well documented, the application of these methods to sediment samples from a contaminated aquifer can offer valuable insights into the mineralogical associations in the bulk sample and their relation to As concentrations. To the best of our knowledge, the application of thermal treatment for analyzing the sedimentary and mineralogical properties that influence the association of As in the sediments within contaminated aquifers was not previously explored. The visual and spectroscopic properties resulting from the

thermal treatment of sediment from areas prone to high groundwater As may provide a simple and inexpensive technique for understanding the behavior of sedimentary As and to quickly constrain relative aqueous As concentrations. The goal of this study is to evaluate the mineralogical associations of sediments collected from an As-contaminated aquifer in Bangladesh, using thermal treatment and spectroscopy techniques to help elucidate the potential availability and mobility of the solid-phase As within the sediments.

2. Methods

2.1. Study Site

The Bengal basin is drained predominantly by the Ganges, Brahmaputra, and Meghna Rivers, which together create the world's largest fluvio-deltaic system [57]. The basin is topographically constrained by the uplifting Himalayan mountains to the north, the Burma Arc fold belt to the east, and the topographically elevated Indian craton to the west [58,59]. The ongoing collision of the Ganges–Brahmaputra delta with the Burma Arc causes active tectonic subsidence in the basin, serving as the topographically preferred pathway for the rivers draining the Himalayas [60]. The Bengal basin is filled with quaternary fluvial deposits, which can be classified into two major units: older, oxidized Pleistocene sediments containing low As groundwater, and more recent Holocene sediments associated with higher groundwater As concentrations [61]. In the time since the last glacial maximum, the rapid sedimentation deposited between 50 and 90 m of intertwined silt, clay, and sand layers, which compose the Holocene aquifers of the Bengal basin [62,63].

In this study, sediment samples from the riverbank and its adjacent aquifer were collected along the Meghna River near the village of Nayapara (23.7° N, 90.7° E) within the Narayanganj district approximately 30 km east of Dhaka. A detailed description of the study site and properties of the sediment samples are described elsewhere [24,64]. The site consists of riverbank sands (0–3 m below ground level, bgl) composed of fine sand, a silt layer (3–7 m bgl), and a 29 m thick medium sand unit (7–36 m bgl) that comprises the shallow aquifer. A clay aquitard underlies the shallow aquifer at 37 m bgl. For this study, samples were taken from each of the lithological units and are herein referred to by their abbreviated lithologies as follows: riverbank sand (RBS), silt layer (SLT), aquifer sand (AQS), and clay aquitard (CLY). The RBS samples (~1 m below ground level, bgl) were collected as pristine sediment cores using a direct push sediment probe (AMS Inc., American Falls, ID, USA) (n = 2). In contrast, discrete depth samples from the SLT (6 m bgl), AQS (23 m bgl), and CLY (37 m bgl) were collected as drill cuttings by the hand flapper method (n = 6) [65]. The properties of a large amount of sediment samples from this site were thoroughly characterized in [24] for elemental composition, particle size distribution, organic matter content, and for the inorganic and organic water-extractable properties. The results of the study show that the chemical properties of the samples from within each lithology (RBS, n = 32; SLT, n = 3; AQS, n = 13; and CLY, n = 2) were homogeneous. However, the sediment properties varied between the different lithologies. For this study, we chose eight well-characterized representative sediment samples from the various lithologies (RBS, SLT, AQS, and CLY) for further mineralogical evaluation. All samples used in this study were stored in Mylar Remel® bags with an O_2-absorbent pouch and kept at −7 °C until analysis. The site was chosen based on reports of high As and Fe groundwater concentrations in the region [66–68], and the previous identification of tidal activity and As enrichment in the riverbank sediments [69–73].

2.2. Sample Preparation and Thermal Treatment

Two samples from each of the four lithologies (RBS, SLT, AQS, and CLY) were chosen for the analyses. The D10 grain size (10th percentile) of each of the samples was calculated following the particle size analysis results of the samples, which is described in detail in Varner et al. [24]. The samples were dried in an N_2 environment and then powdered using an agate pestle and mortar. An aliquot of each sample was then placed in a furnace preheated to 600 °C for a duration of three hours. In total, there were two untreated samples

from each lithology and an aliquot of each sample underwent the thermal treatment for a total of 16 samples prepared for the analyses (n = 8 untreated, n = 8 thermally treated).

2.3. Fourier Transform Infrared Measurements

A single-beam Fourier transform infrared spectrophotometer (IRSpirit, Shimadzu Corporation, Kyoto, Japan) was used for the collection of the mid-infrared spectra of the sediment samples by the attenuated total reflectance (ATR) technique between the 4000 and 650 cm^{-1} range. The ATR cell was equipped with a germanium-coated KBr beam splitter and a QATR-S diamond crystal attachment (45° angle of incidence). Data were collected as the average of 64 scans with a resolution of 4 cm^{-1}, and each resulting spectrum was automatically corrected for the ATR method by the instrument assuming a refractive index of 1.5 for the sample. A background reading was collected between samples and subtracted from subsequent measurements. The resulting FTIR spectra were baseline corrected and smoothed in Spectragryph (v1.2.16.1).

2.4. Reflectance Spectroscopy

Color is a conspicuous feature of Fe-oxy(hydr)oxides and diffuse reflectance (DR) spectroscopy techniques were extensively used to quantify the color content for the characterization of iron-oxide mineral content in natural sediment samples [50,74,75]. For this work, the DR spectrum of both the untreated and treated samples was collected using a CM-600d spectrophotometer (Minolta Corp., Tokyo, Japan) and was recorded relative to a standard $BaSO_4$ white plate. The observer angle of the spectrophotometer was set to 10° with the exclusion of direct reflection specular components. Measurements were taken using an illuminant source of D65, a standard illuminant corresponding to midday light and to a color temperature of ~6500 K. For DR measurements, the sample was placed in a cut paper cup (diameter = 2.5 cm) and was smoothed and covered with clear polyethylene wrap to provide a planar surface for measurements. Each sample data spectrum is the automated average of five readings. A standard white plate was measured between the collection of each sample spectrum. The first transform derivative of the reflectance spectra (ΔR) was then obtained by taking the difference of the % reflectance of the two adjacent 10 nm wavelength measurements for a given point.

2.5. X-ray Fluorescence

The elemental concentrations of As were measured by X-Ray fluorescence (XRF) in each of the 16 samples using a Niton XL3t 500 GOLDD handheld XRF spectrometer (Thermo Scientific, Waltham, MA, USA, Cat no. XL3TGOLDDPLUS). The analysis settings were employed for the optimum measurement of heavy elements in soils with a SiO_2 matrix. To collect the data, the analyzer was placed directly on each sample and analyzed for 120 s (60 s main filter, 30 s low filter, and 30 s light filter) at a maximum voltage of 40 kV. The XRF measurements for As of standard reference materials (NIST 2709a, NIST 2780, and CCRMP Till-4) yielded an average relative percent difference of 6.4% from the certified values, well within the accepted range of error (±20%) for the instrument. A conservative method detection limit (MDL) was determined as three times the instrument's 2σ measurement error measured in samples with none or trace amounts of each analyte, as defined by the EPA SW-846 method 6200 definition of detection limits for XRF [76].

3. Results

3.1. FTIR

The FTIR results of the untreated samples between 1400 and 400 cm^{-1} reveal spectra with five prominent peaks centered at ~1030, ~790, ~690, ~530 cm^{-1}, and ~470 cm^{-1}. The highest absorbance for all peaks was recorded in the clay and was lower for all peaks in the sand samples (Figure 1a). The vibrational assignments of the peaks found in this study are presented in Table 1. Briefly, the assignment of the peaks at ~1030, ~790, ~690, ~530 cm^{-1}, and ~470 cm^{-1} are primarily attributed to antisymmetric Si-O-Si stretching,

symmetric Si-O-Si stretching, perpendicular Si-O stretching, Si-O-Al^{VI} bending, and Si-O-Si bending, respectively [49,77]. Smaller secondary peaks may provide diagnostic information and occur in the FTIR spectra at ~915 cm^{-1} as a shoulder, a broad band between 800 and 740 cm^{-1}, at 435 cm^{-1}, and are attributed primarily to $\delta(Al_2OH)$ deformation, Fe(III)Mg-OH bending or Al^{IV}-O-Si in-plane vibration, and Si-O-Si bending, respectively [49,77].

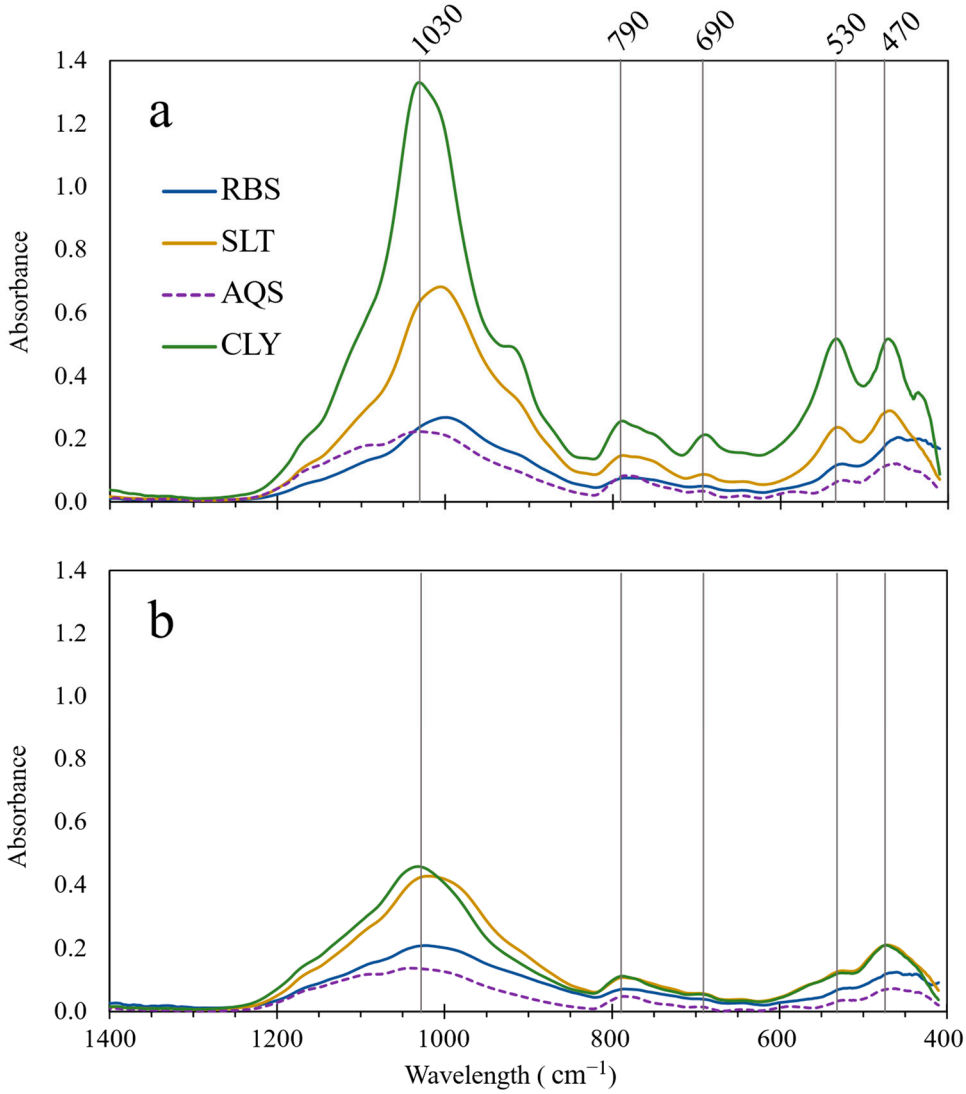

Figure 1. (**a**) FTIR spectra between 1400 and 400 cm^{-1} of the untreated sediment from the riverbank sand (RBS), silt (SLT), aquifer sand (AQS) and the basal clay (CLY); (**b**) FTIR spectra of the sediment subjected to thermal treatment at 600 °C.

The thermal treatment resulted in a considerable decrease in the intensity across all wavelengths (Figure 1b). Changes caused by thermal treatment can be easily assessed by the difference between the spectra of the untreated and thermally treated samples (Figure 1). The greatest amount of change caused by the thermal treatment was observed in the peaks located at ~1022, 912, between 800 and 750, 689, 530, and 464 cm^{-1}, associated mostly with various Si-O and Al-O vibrations. Thermal alterations were most noticeable in the clay and silt samples and produced minimal changes in the sand samples as seen by the relatively flat absorbance in the differential FTIR spectra (Figure 1, Table 1). The spectra of the treated samples retained a broad peak at ~1030 cm^{-1}, a small peak between 800 and 700 cm^{-1}, and produced a broad sloping peak at 460 cm^{-1} in lieu of the two distinct peaks in the original sample spectra at 534 cm^{-1} and 467 cm^{-1} (Figure 1a,b).

Table 1. Assignment of the vibrational peaks in the FTIR spectra between 1400 and 400 cm^{-1}. Data for the table were constructed from Farmer [77] and Madejová et al. [49] unless stated otherwise.

Peak (cm^{-1}) This Study	Vibration Assignment	Reported Peak Center (cm^{-1})	Mineral Associations
1029	Asym. Si-O-Si Stretching	1000–1040	Kaolinite, illite, smectite, muscovite
940–890	$\delta(Al_2OH)$	915–935	Kaolinite, illite, muscovite
	δ-OH deformation	888–916 [a, b, c, d]	goethite, hydrohematite
800–740	Sym. Si-O-Si stretching	798 and 780	Quartz doublet
	γ–OH deformation	795 [a, b, c, d]	Goethite
	$Fe^{3+}Mg$-OH bending	765756	Smectite
	Al^{IV}-O-Si in-plane		Illite
691	Perpendicular Si-O	695	Kaolinite, quartz
534	Si-O-Al^{VI} bending	540–524	Kaolinite, smectite, illite
	Fe-O	530–536 [a, b]	Hematite, goethite
467	Si-O-Si bending	470	Kaolinite, smectite, illite, muscovite
	Fe-O	452–460 [a, b, c]	Hematite, goethite
435	Si-O-Si bending	428–443	Smectite, illite, muscovite

[a] Ruan et al. [47]; [b] Chen et al. [78]; [c] Prasad et al. [79]; [d] Margenot et al. [80].

3.2. Diffuse Reflectance Measurements

Consistent with previous studies, the reflectance spectrum of sediments with deeper brown and orange hues is more elevated in the 550 to 700 nm range than that of grey sediment, which typically displays a flatter reflectance spectrum in this range (Figure 2a,b) [65,81]. In the fresh, untreated samples, the AQS samples displayed the highest values with an apparent slope in the DR spectra throughout the 400 to 700 nm range as opposed to the RBS (Figure 2a) and the SLT and CLY, which showed similar values (Figure 2b). Thermal treatment of the samples at 600 °C caused an increase in brown-orange hues in all samples as reflected in the high gradient of the DR spectra between 400 and 700 nm (Figure 2a,b).

The ΔR, or first-transform derivative of the reflectance, is highly reproducible and provides indicative information on Fe-oxide mineralogy. For example, Horneman et al. [65] found that the ΔR at 520 nm is negatively correlated to the Fe(II)/Fe(Total) content in the sediment and can be used as a proxy for Fe(III); other authors noted that the ΔR spectra are sensitive indicators for hematite and goethite with peaks occurring between 555 and 575 for hematite and two peaks between 420–430 and 480 to 530 for goethite [82–85]. The ΔR spectra of the untreated and thermally treated sediment samples show contrasting results (Figure 2c,d). The ΔR at 520 nm of the untreated samples was typically lower than the ΔR at 520 nm of the thermally treated counterparts (Table 1), indicating an increase in the proportion of Fe-oxides. In the SLT and CLY samples, the ΔR at 520 nm increased an average of 53 ± 3.4% following the thermal treatment (Figure 2c), whereas no noticeable changes in the ΔR at 520 nm were observed in the sand samples from the same treatment (Figure 2d). All untreated samples lack the hematite peak centered around 560 nm; rather, peaks at 420 and 500 nm indicate the presence of goethite in the samples, specifically in the RBS and AQS. The thermal treatment caused the goethite peaks at 420 and 500 nm to diminish and produced a large peak between 550 and 560 nm, indicating the formation of hematite (Figure 2c,d). Furthermore, a new peak at 450 nm formed in the thermally treated samples, which is a product of the thermal transformation of goethite to hematite in the DR spectra [81]. The hematite peak of the SLT and CLY samples showed a lower intensity and was centered at 550 nm (Figure 2d), whereas that of the RBS and AQS showed a higher intensity and was centered at 560 nm (Figure 2c).

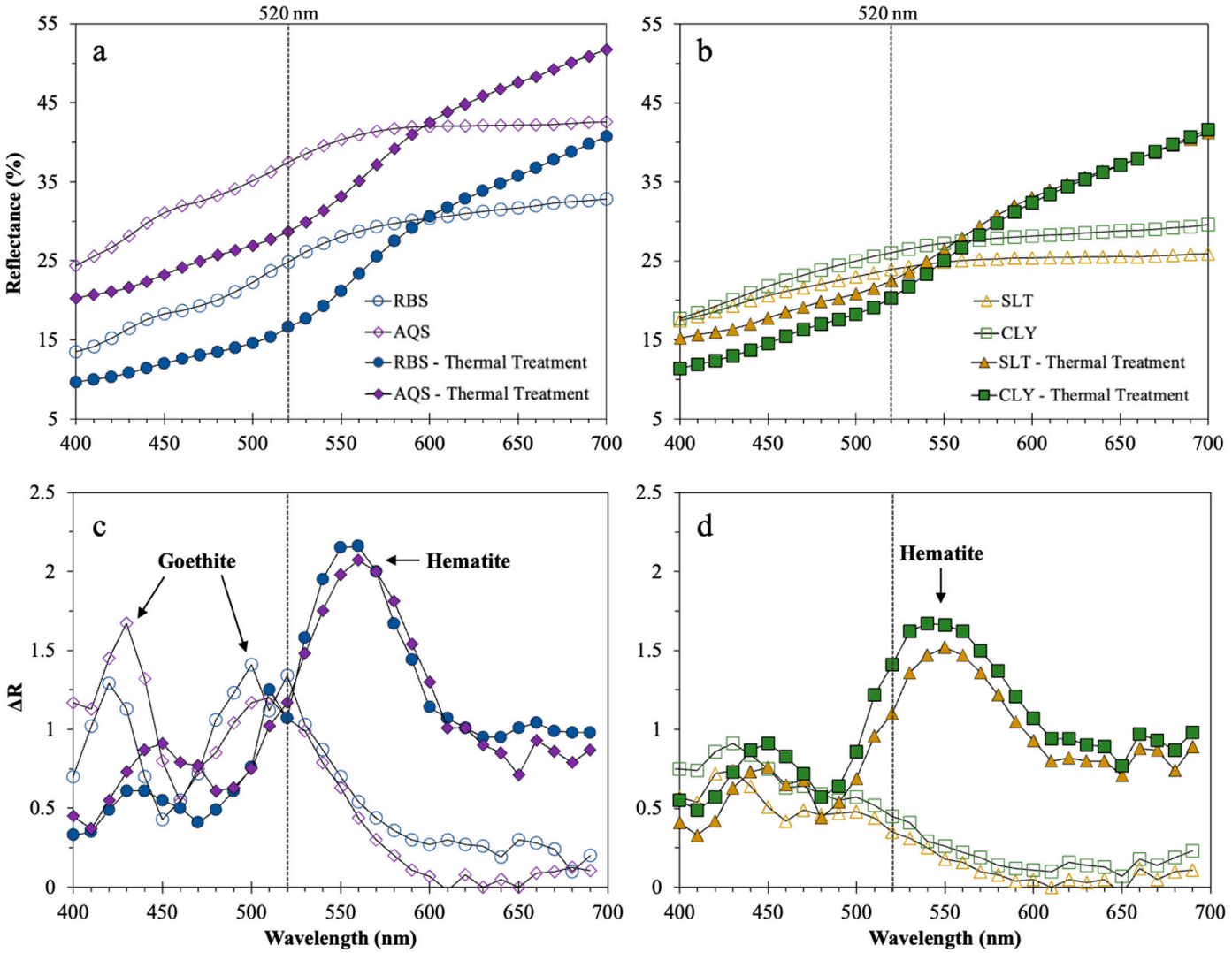

Figure 2. Diffuse spectral reflectance data for the sand samples (**a**) and the silt and clay samples (**b**); calculated ΔR values for the sand samples (**c**) and the silt and clay samples (**d**). The vertical dashed line indicates 520 nm. The open symbols represent the untreated samples, and the filled symbols represent the thermally treated samples.

3.3. Elemental Concentrations

Initial concentrations of Fe were higher in all samples before thermal treatment. On the other hand, the effects of thermal treatment on the concentrations of As were restricted to the finer-grained CLY samples, and to a lesser extent the SLT samples, which decreased following the thermal treatment (Table 2). The As concentrations in the AQS samples were above the instrument detection limit of 1.1 mg/kg. However, all measurements of AQS samples were lower than the MDL of 3.5 mg/kg. The initial concentrations of As in the RBS, SLT, AQS, and CLY (6.0, 2.3, <1.3, 11.4 mg/kg, respectively) were comparable to values previously reported for similar sediments at the site [24]. In general, the concentrations of the untreated sediment are within the ranges of previously reported sedimentary concentrations using XRF along the Meghna Riverbank and adjacent floodplain aquifer [23,70,73]. The As concentrations decreased after the thermal treatment by an average of 1.4, 2.3, 1.1, and 6.25 mg/kg for RBS, SLT, AQS, and CLY, respectively. However, given the analytical uncertainties associated with the handheld XRF and the reported standard deviations, only the CLY and one of the SLT samples showed a notable decrease that can be attributed to the thermal treatment. However, the concentrations of Fe in the RBS, SLT, AQS, and CLY

(29, 37, 6, and 37 g/kg, respectively) were higher than the measurements following thermal treatment (26, 31, 5, and 20 g/kg, respectively).

Table 2. Results showing the first transform derivative of the reflectance at 520 nm and the measured concentrations of As and total Fe in the samples before and after the thermal treatment. Results in parentheses are below the MDL.

	As (mg/kg)		Total Fe (g/kg)		ΔR at 520 nm	
	Untreated	**Treated**	**Untreated**	**Treated**	**Untreated**	**Treated**
RBS-1	5.42 ± 1.09	4.42 ± 1.19	30.04 ± 0.82	24.61 ± 0.91	1.02	1.25
RBS-2	6.61 ± 1.21	4.80 ± 1.16	28.84 ± 0.81	26.69 ± 0.77	0.72	0.75
SLT-1	8.13 ± 1.27	6.71 ± 1.39	40.08 ± 0.91	32.29 ± 0.85	0.45	0.89
SLT-2	6.39 ± 1.34	3.85 ± 1.15	34.03 ± 0.90	29.47 ± 0.79	0.44	0.96
AQS-1	(1.33) ± 1.00	(1.16) ± 0.48	5.36 ± 0.31	4.46 ± 0.27	1.01	1.02
AQS-2	(1.33) ± 0.87	(1.06) ± 0.87	6.57 ± 0.34	5.31 ± 0.29	1.2	1.02
CLY-1	11.49 ± 1.36	4.66 ± 0.74	37.18 ± 0.92	14.28 ± 0.46	0.6	1.25
CLY-2	11.22 ± 1.34	6.25 ± 0.98	36.54 ± 0.92	24.71 ± 0.67	0.52	1.22

4. Discussion

4.1. Spectral and IR Changes in Clay Mineralogy in Response to Thermal Treatment

The FTIR spectra are often dominated by the most abundant vibrational frequencies in the spectra. The mineral structures of clays are especially sensitive to IR spectroscopy since the predominant vibrations in the near-infrared range (hydroxyl groups and the Si-O network) are enhanced in clay minerals (i.e., O-H, Si-O, Al-O, Fe-O, and Mg-O bonds) [45–47]. Given that Al, Fe, and Si make up most of the elemental composition of the RBS, SLT, AQS, and CLY sediments (average = 88%, 84%, 92%, and 85%, respectively) [24], the FTIR spectra are interpreted in the context of these abundant elemental concentrations.

The FTIR spectra of the untreated sediment displayed peaks that are characteristic of 1:1 and 2:1 layered clay minerals (Figure 1a) [49,77,86,87]. A diagnostic peak of clay minerals occurs from the strong Si-O-Si vibrations centered at ~1030 cm^{-1}; the shape of this dominant peak may provide further distinction of the clay minerals present. For example, the extensive substitution within the sheets of 2:1 clay minerals (i.e., smectite, illite, and muscovite) results in a broadening of this peak centered at 1030 cm^{-1}, which may obscure the two distinct Si-O vibrations produced by kaolinite at ~1035 cm^{-1} and 1010 cm^{-1} [49,77]. However, the occurrence of kaolinite is confirmed by the peak at 691 cm^{-1} from perpendicular Si-O vibrations in the mineral lattice of kaolinite (in conjunction with an absorbance band at ~755 cm^{-1}). On the other hand, the presence of smectite is confirmed by a diagnostic band near 430 cm^{-1} attributed to Si-O-Si bending, whereas a band near 756 cm^{-1} resulting from Al-O-Si in-plane vibration is diagnostic of the structure of illite minerals [77]. Furthermore, the untreated FTIR spectra of the samples, specifically in CLY, showed a slight shoulder between ~940 and 915 cm^{-1}, which is often attributed to the OH bending of inner-surface OH groups of Al_2OH in kaolin minerals and the δ((Fe)Al_2OH) bending of substituted illites and smectites [49]. Although not quantified, the FTIR spectra indicate that illite, smectite, and kaolinite contribute to the majority of the clay mineral assemblages in the riverbank and aquifer sediments.

The thermal treatment of the samples at 600 °C caused noticeable changes in the spectroscopic properties of the sediment. The most notable change was the overall diminishing in the peaks located at ~1022, 912, between 800 and 750, 689, and 530 in the FTIR spectra (Figure 1), which is characteristic of kaolinite and 2:1 layered clay minerals such as smectite and illite in response to elevated temperatures [88]. These peaks are primarily associated with the common functional groups of clay minerals, including the bending vibrations of Si and Al networks and OH deformations at ~912 cm^{-1} (Table 1). The decrease in absorbance can be attributed to the partial decomposition of the clay mineral structures resulting

from dehydroxylation, which occurs at temperatures between 100 and 500 °C as well as between 100 and 650 °C for kaolinite and both illite and Fe-smectite, respectively [54,55,89]. Evidence for the dehydroxylation of the clay minerals in the samples following the thermal treatment can be observed by the decrease in the band attributed to the Al-OH bending vibration at ~930 cm^{-1} (Figure 1), which was accompanied by a decrease in the Al-OH stretching region for kaolinite and illite at ~3620 cm^{-1} (not shown). The removal of OH from the clay mineral's structure results in a significant decrease in the vibrations associated with the OH group, although some minerals, such as micas, only begin to dehydroxylize at temperatures above 700 °C [89,90]. Following dehydroxylation, the partial collapse or deformation of the clay mineral structure diminishes the bands attributed to the Si- and Al-O of phyllosilicate minerals, primarily near 1030, 690, and 530 cm^{-1}. It is relevant to note that the majority of the organic matter trapped in the sediments would be volatilized during the thermal treatment at 600 °C. However, the contribution of organic molecules in the FTIR spectra cannot be distinguished as the vibrations from the organic molecules are likely obscured by the more dominant bands produced by clay minerals in the samples.

These findings are further supported by the chemical index of alteration (CIA) of the bulk samples (Figure 3). As defined by Nesbitt and Young [91], the CIA provides the extent of weathering of plagioclase and K-feldspar for their aluminous weathering products (i.e., clay minerals), which is determined as CIA = $[Al_2O_3/(Al_2O_3 + CaO^* + Na_2 + K_2O)] \times 100$, where the elements are represented by their molecular proportions and CaO* represents CaO in the silicate fractions. Higher CIA values, approaching the maximum value of 100, represent more extensive chemical weathering under more humid conditions with a chemical composition closer to pure kaolinite. Using the elemental concentrations of the same samples presented in Varner et al. [24], the bulk sediment CIA values of the RBS, SLT, AQS, and CLY samples averaged 65, 69, 61, and 78, respectively. These values indicate only a moderate amount of chemical weathering, consistent with the rapid erosion and recent deposition of the Holocene aquifers of Bangladesh. The CLY sample is shown to have the lowest Na/K ratio compared to the AQS, SLT, and RBS samples, which are associated with more intense weathering processes, indicating more mature sediments. The rapid deposition of the Holocene sediments resulted in an overall low transport time, somewhat limiting the exposure of sediments to weathering processes. For example, the Pleistocene aged Dupi Tila clay underlying the Holocene deposits in eastern Bangladesh has a CIA value averaging 93% [92]. A weathering line parallel to the A-CN line in the A-CN-K ternary plot reflects the retention of K and a higher mobility of Na and Ca during chemical weathering, resulting in higher proportions of illite in weathered sediments (Figure 3) [93]. Here, the CIA is determined from the bulk elemental composition of the sediments rather than only the clay fractions. However, based on the FTIR and CIA results, the predominant clay minerals in these sediments are illite, smectite, and, to a lesser extent, kaolinite.

These findings are similar to previous studies that used X-ray diffraction analysis to identify the occurrence of feldspars and clay minerals such as kaolinite, micas, smectite, and illite in aquifer sediment along the Meghna River [19,73] and to studies that reported illite as the most abundant clay mineral in Bengal basin river sediments, followed by smectite, kaolinite, and chlorite [94–96]. Similarly, in a study examining the properties of clays from various parts of southeast Bangladesh using both XRD and FTIR analyses, Dewan et al. [97] found that illite, kaolinite, and quartz were the dominant minerals with only minor phases of oxides present, such as goethite or hematite. The occurrence of these phyllosilicate minerals may play a prominent role in regulating the release and fate of As in contaminated aquifers. The role of clay minerals, such as biotite and muscovite, was implicated in regulating dissolved As concentrations in West Bengal, India [32,98]; whereas in Bangladesh, chlorite was suggested as a prominent source of As pollution in the shallow aquifers [20]. A study in the Mekong Delta, Vietnam by Huyen et al. [34] suggests that kaolinite and phyllosilicate minerals play an equally significant role in regulating dissolved As concentrations as the role played by Fe-oxides in the aquifer. The roles that kaolinite, illite, and other phyllosilicates have in the immobilization and transportation of As in

contaminated aquifers should be further investigated under a variety of naturally occurring conditions to better understand the effects of these common minerals on the dissolved As concentrations.

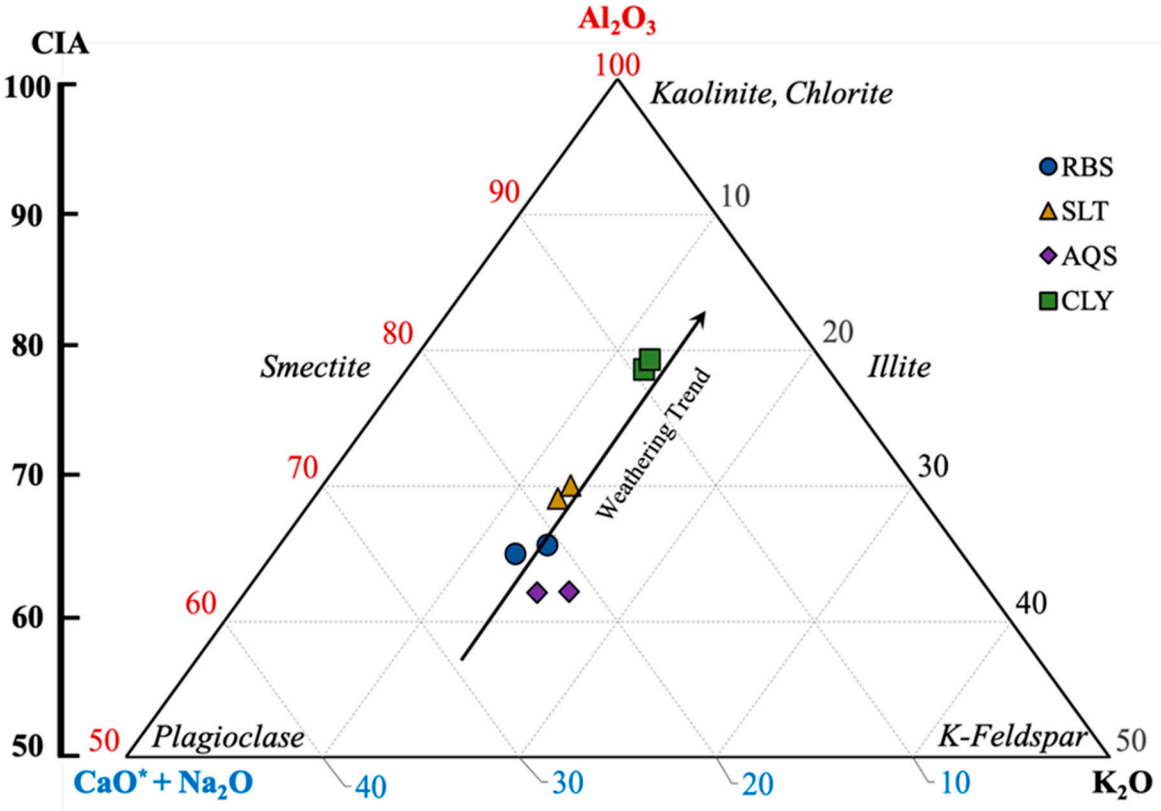

Figure 3. A-CN-K ternary plot as defined by Nesbitt and Young [91] showing the composition of the untreated sediment samples along with the correlated mineral hosts in italics. The elemental concentrations used to calculate the CIA values are from the same sediment samples that were presented in Varner et al. [24].

4.2. Fe Mineralogy and Transformations from Thermal Treatment

Numerous studies examined the relationships between As and Fe-oxide minerals in natural sediments with a particular focus on the reductive dissolution processes of Fe-oxides. These investigations utilized methods such as kinetic studies to determine the rates of As release from different Fe-oxides [99,100], sequential extractions to understand the partitioning of solid-phase As among mineral phases [101], and X-ray absorption spectroscopy to identify the speciation and associations between As and Fe-oxide phases [71,102]. While these methods provided valuable insights, they can be time-consuming and expensive. Alternatively, simple spectroscopic techniques combined with thermal treatment may offer a rapid means to estimate bulk properties of Fe-oxides and Fe-bearing minerals in samples. The thermal treatment of sediments also indicates the nature of Fe in the sample as both Fe-oxides and the structural Fe in clay minerals undergo transformations as the temperature increases. For example, the direct dehydroxylation of goethite and transformation to hematite species begins at 200–280 °C [47,53,55,103,104], whereas for Fe associated in the structure of clay minerals, this transformation must be preceded by the structural deformation and collapse of the mineral lattice above 400 °C [81]. The oxidation of structural Fe(II) is accelerated by thermal treatment [42]. The Fe that can no longer be accommodated in the thermally altered silicate structures will then proceed to form hematite as the temperature increases [55,56,105,106]. Murad and Wagner [55] found that divalent Fe was absent in illite above temperatures of 300 °C, whereas Fe(III) increased from 350 to 450 °C, causing

a change in color to a deeper reddish-brown hue. This process is likely the cause of the dramatic increase in the reddish-brown hues of the thermally treated SLT and CLY samples.

Although the vibrational frequencies of clay minerals may obscure the diagnostic bands of Fe-oxides, previous use of FTIR for Fe-oxide phase transformation suggests that absorbance bands are a good indicator of the migration of excess hydroxyl units from goethite to hematite [107]. In the FTIR spectra, the peaks that are typically diagnostic of hydroxyl deformations in goethite (δ-OH deformation at 900 cm^{-1} and γ–OH deformation at 795 cm^{-1}) were observed to decrease in all samples following thermal treatment (Figure 1) [79,108]. Furthermore, the decrease in the shoulder at 916 cm^{-1} and the broadening and reduction in the absorbance band at 534 cm^{-1} in the FTIR spectra of the treated samples is indicative of the dehydroxylation of goethite and of the OH substitution for O in the Fe-O bond of goethite and hydrohematite, respectively [47,78]. The removal of OH from the goethite structure as the temperature increases causes the band centered at 534 cm^{-1} to shift to lower wavelengths and broaden. The broadening of this peak is observed in the thermally treated samples from ~600 to 452 cm^{-1} and is consistent with previous work using FTIR techniques to investigate the thermal transformation of both natural goethite and Al-substituted goethite to hematite [47,79,109].

Diffuse reflectance spectroscopy in the 400 to 700 nm range is sensitive to minute amounts of Fe in the samples and can be used to differentiate between Fe(II) and Fe(III) in the samples [65]. In the untreated sediment, Fe(III) was observed in the RBS and AQS samples but was not readily apparent in the finer-grained SLT or CLY samples. The thermal treatment caused the proportions of Fe(III) to increase in all samples as indicated by the increase in the slope gradient in the DR spectra (Figure 2a,b). The ΔR spectra of the untreated samples showed the presence of Fe(III) as goethite in the RBS and AQS samples (peaks at 420 and 500 nm), whereas the finer-grained SLT and CLY samples did not contain any discernible peaks due to the relatively low proportions of Fe(III). However, following thermal treatment, the presence of hematite (~560 nm) was observed in the ΔR spectra of all samples (Figure 2c,d) [65,84,85]. Interestingly, the hematite peak in the sand samples was located at 560 nm whereas the hematite peak in the thermally treated SLT and CLY samples was shifted down to 550 nm and exhibited a lower reflectance value despite higher initial bulk Fe concentrations. The shift of the hematite peak may indicate the initial Fe mineralogy of the samples. The sands experienced the direct transformation of goethite to hematite. In contrast, the Fe in the SLT and CLY was incorporated as structural Fe(II), which was only transformed to hematite following the structural deformation of clay minerals (Figure 2d).

These proposed mechanisms of hematite formation are supported by the increase in the ΔR value at 520 nm after thermal treatment, which shows minimal changes for the sand samples (0.02) compared to that of the silt (0.48) and clay (0.68), indicating a greater increase in the proportion of Fe(III) in SLT and CLY [65]. The ratio of hematite relative to goethite should increase with increasing temperature. However, in the SLT and CLY samples where the Fe was primarily present in the structure of clay minerals, the hematite was produced indirectly from the degradation of clay minerals. Here, we show that the thermal treatment of sediments, combined with DR and FTIR spectroscopy, helps determine the relative proportions of Fe in clay minerals as opposed to oxide coatings in sediment. The sand samples contained Fe as Fe-oxides/hydroxides coating sediment grains, whereas the Fe of the finer-grained SLT and CLY samples was present as structural Fe within clay minerals.

4.3. Mineral Associations of As in the Sediment

The initial concentrations of As in RBS, SLT, AQS, and CLY (6.0, 2.3, <1.3, 11.4 mg/kg, respectively) decreased after thermal treatment by an average of 1.4, 2.3, 1.1, and 6.3 mg/kg, respectively (Table 2). Removal of As during heating could be attributed to the volatilization of As. The extent of As volatilization is more complete from rapid combustion than under slow heating conditions [110], and multiple studies investigating coal combustion note that As volatilization increases with temperature, with around 80% of As being volatilized at

temperatures of ~900 °C [110–114]. At temperatures less than 600 °C, organic-bound arsenic is readily volatilized [114], and any exchangeable As and As bound to poorly crystallized Fe-Mn (hydr)oxides are volatilized at temperatures lower than 1000 °C [110,115]. In pure clay samples (kaolin), Gray et al. [116] found that between 22 and 40% of As was volatilized at temperatures of 520 to 1120 °C. The removal of higher amounts of As from the thermal treatment at 600 °C, a temperature at which the majority of organic material is volatilized, in the SLT and CLY samples suggests that a larger portion of the As in these sediments is associated with OM, specifically in CLY.

The association of As with organic-rich clays is well documented in the Bengal basin [4,11,23,26]; these deposits are often dominated by the co-occurrence of OM, clay minerals, and amorphous oxide minerals, which provide an abundance of sorption sites to promote the adsorption and accumulation of As [18]. Despite the consistent As enrichment observed in the clay and silt layers, the association of As and OM is not clear. It is apparent, however, that the mobilization of As from these sediments is likely regulated by the characteristics of the sedimentary OM associated with the finer-grained sediments. A recent study in the Datong basin in China by Liu et al. [117] suggests that sedimentary OM rich in aliphatic compounds is preferentially degraded and promotes the reduction in As-bearing Fe minerals. Similarly, at this study site, the sedimentary OM in the SLT contains relatively high proportions of aliphatic polysaccharide moieties, which can sustain the reductive dissolution of Fe-oxides, whereas the CLY at the study site is enriched in recalcitrant, aromatic OM that favors the formation of soluble ternary As-Fe-OM complexes (Varner et al., 2023, In Prep).

Furthermore, the incorporation of Fe in the mineral structure of clay minerals contributes to the elevated concentrations of Fe in the clay layers of the Bengal basin, as structural Fe(II) accounts for more than 50% of the mass of Fe in the subsurface [42]. Because the ΔR at 520 nm may be used to indicate the proportions of Fe(III) in a sample [65], and the thermal treatment transformed the structural Fe(II) in clay minerals to hematite phases, the difference in the ΔR at 520 nm values of the untreated and thermally treated sediments may be used as a proxy for the transformation of Fe-bearing clay minerals in the samples. The occurrence of structural Fe(II) in clay minerals is further reflected by the correlations between both grain size and CIA, with the difference of the ΔR at 520 nm caused by thermal treatment (R^2 = 0.92, p = < 0.001 and R^2 = 0.85, p = 0.001, respectively), which transforms structural Fe(II) to hematite phases at elevated temperatures (Figure 4a,b) [24]. Following the thermal decomposition of OM and clay minerals, it is likely that any associated As was liberated and subsequently volatilized during thermal treatment, whereas the structural Fe was transformed to hematite phases. An indication of this process is shown by the high correlation between the initial As concentrations and the difference in the ΔR at 520 nm of the samples before and after thermal treatment (R^2 = 0.80, p = 0.003), which is a proxy for the amount of Fe(II) incorporated within the structure of clay minerals (Figure 4c). This positive correlation of sedimentary As concentrations with the amount of structural Fe(II) suggests that As is primarily associated with clay minerals within the finer-grained sediments.

The coexistence of elevated Fe-hydroxides and OM along with As is a result of the affinity of Fe for both As and OM. However, phyllosilicates, such as kaolinite and illite, are known to incorporate or adsorb As [32,34]. The thermal treatment of the sediments and the resulting loss of As in the finer-grained samples suggests that large portions of solid-phase As are associated with these clay minerals or OM. Additionally, the abundant amount of initial As in natural clays limits their potential as potential sorbents [118]. However, the oxidation of Fe in illite and kaolin from the heating process may calcinate the sample and makes for a simple and effective modified sorbent for As removal [119]. While the release of As under environmental conditions in the aquifers of Bangladesh may be regulated by Fe-oxide reduction, OM and phyllosilicate clay minerals may directly regulate the mobility of much of the As in the solid phase. The associations between As and finer-grained sediments are clear. Therefore, further investigations to understand the interactions between specific

clay minerals and organic functional groups within the clay layers and their effect on the attenuation or release of As would advance the understanding of As in deltaic aquifers.

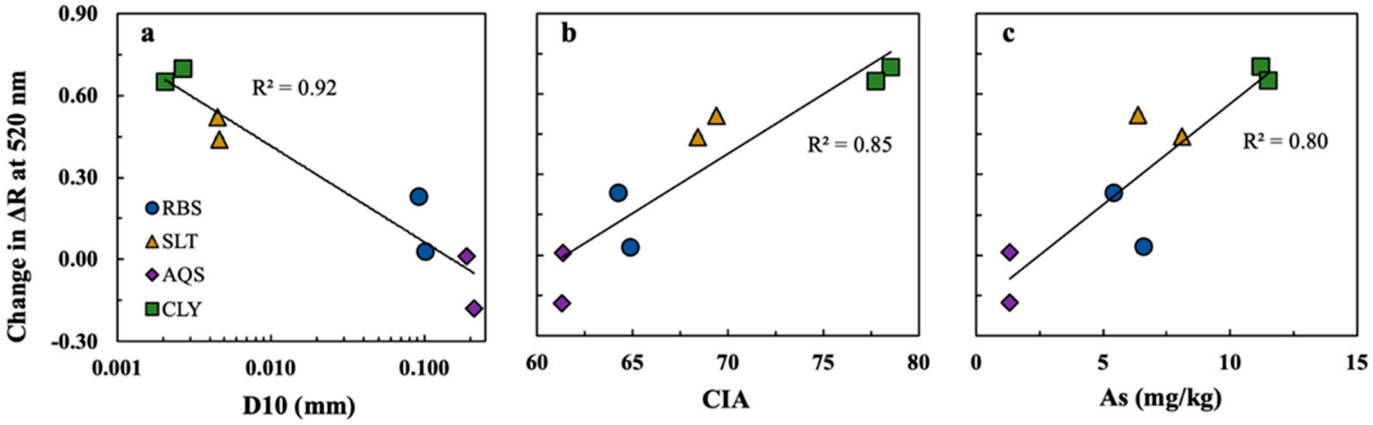

Figure 4. Correlation between the difference of the ΔR at 520 nm in the untreated and thermally treated sediment for each measured sample and (**a**) the D10 grain size; (**b**) the CIA value; and (**c**) the sedimentary concentration of As in the untreated samples. The difference of the ΔR at 520 nm serves as a proxy for the structural Fe in the sample that can be transformed to hematite phases at elevated temperatures. The D10 grain size and elemental concentrations for the CIA are presented in Varner et al. [24].

4.4. Implications of Study and Need for Future Work

This study advances our understanding of the geochemical processes along the Meghna River, where, as a developing long-term study site, the porewater chemistry was characterized [73], the subsurface lithology was determined using electrical resistivity methods [64], and the elemental composition and organic matter content of the sediments were characterized and evaluated in relation to the mobilization and sequestration of As [24]. In this study, the bulk mineralogical associations of As were determined in the sediments by FTIR and DR techniques alongside thermal treatment to induce diagnosable changes in the sediment. This study highlights the significance of Fe-bearing clay minerals in controlling the distribution of sedimentary As distribution in a naturally contaminated aquifer, suggesting their comparable importance to Fe-oxides in determining As partitioning. Although previous studies suggested the important role of clay minerals in As release and immobilization in the Bengal basin [20,32,120], the associations and processes between clay minerals and As in these aquifers remain uncertain. This study establishes a strong correlation between the proportions of As and the proportions of structural Fe(II) in common clay minerals such as kaolinite and illite, which are abundant in the organic-rich fine-grained deposits of the Bengal basin. Common spectroscopic techniques coupled with thermal treatment enable rapid quantification of bulk sediment properties, such as structural Fe(II) proportions and relative goethite/hematite ratios, providing qualitative descriptions of sedimentary As associations. Similar spectroscopic analyses were traditionally used in the fields of anthropology and materials science for identifying the original mineralogical composition and source of fired clay. This approach can be applied to contaminated sediment sites to assess major mineral hosts regulating As concentrations. However, further research is needed to confirm and expand upon these findings. It should involve a larger and diverse sample size from various geological settings. Additionally, confirming and enhancing the results can be achieved through the utilization of ^{57}Fe Mössbauer spectroscopy, which can quantify the Fe retained by aluminosilicate structures after thermal treatment and provides relevant information on the valence state and site geometry of Fe. A comprehensive confirmation of the study's findings would involve conducting the thermal study alongside DR and Mössbauer spectroscopic analyses.

5. Conclusions

This study employed the use of FTIR and diffuse reflectance to define the mineralogical response of thermal treatments on riverbank and aquifer sediment from a contaminated aquifer along the Meghna River in Bangladesh. To our knowledge, the determination of the sedimentary associations of As in aquifer sediments from Bangladesh using the combined techniques was never implemented despite the known association of solid-phase As with both clay minerals and Fe-oxides in deltaic aquifers. The results highlight the importance of Fe-bearing clay minerals in controlling the distribution of solid-phase As in contaminated aquifer sediments.

Thermal treatment of the samples changed the sediment color to a more reddish-brown hue, with the greatest color change exhibited by the silt and clay samples. The FTIR analyses revealed the presence of clay minerals, such as illite, smectite, and kaolinite samples. Diffuse reflectance measurements showed that the Fe in the sand samples was present as goethite coatings, whereas Fe in the finer-grained silt and clay samples was largely present as reduced Fe within the structure of clay minerals. Initial As concentrations were higher in the clay and silt samples (11.4, 7.3, mg/kg, respectively) than in the riverbank and aquifer sand samples (6.0, <1.3 mg/kg, respectively). Following thermal treatment, As was volatilized in the clay and silt samples with the average concentrations of As decreasing by 52 and 29%, respectively.

The proportions of structural Fe(II) present in the clay minerals correlated both to the initial concentration of As in the sediments and to the proportion of the As removed following the thermal treatment of the sediments. The highly reactive structural Fe(II) in the silt and clay samples may explain the high levels of association documented between Fe, OM, and As within the shallow aquifers of Bangladesh. Whereas the reductive dissolution of Fe-oxides may explain the mobilization of As, these findings imply that clay minerals may strongly regulate the mobility and fate of solid-phase As. However, further research is needed to confirm and expand upon these findings, including evaluating a larger sample size and the use of 57Fe Mössbauer spectroscopy to quantify retained Fe in clay minerals and validate the response to thermal treatment.

Author Contributions: T.S.V.: conceptualization, methodology, validation, formal analysis, investigation, data curation, writing—original draft, and visualization. H.V.K.: conceptualization, methodology, validation, formal analysis, investigation, data curation, writing—review and editing, visualization, and supervision. M.U.B.: methodology, formal analysis, investigation, data curation, writing—review and editing. P.S.K.K.: resources, writing—review and editing, project administration, and funding acquisition. M.B.C.: resources, writing—review and editing, project administration, funding acquisition. S.D.: conceptualization, resources, writing—review and editing, project administration, supervision, and funding acquisition. All authors have read and agreed to the published version of the manuscript.

Funding: This research was funded by the National Science Foundation Hydrologic Sciences grant numbers EAR- 1852652, EAR- 1852653, and EAR- 1940772.

Data Availability Statement: The data presented in this study are available upon request from the corresponding author(s).

Acknowledgments: We acknowledge assistance from Kazi Matin Ahmed for overseeing field logistics and thank Alamgir Hossain, Raya Tarrannum, and Mahmudul Hasan from the University of Dhaka for assistance in the field. We want to thank the UTSA Chemistry Department for providing access to the FTIR instrument and to Department of Geology and Geophysics at Texas A&M University for access to the XRF. Funding was provided to Peter S. Knappett, M. Bayani Cardenas, and Saugata Datta by the National Science Foundation Hydrologic Sciences grant numbers EAR- 1852652, EAR-1852653, and EAR- 1940772, respectively.

Conflicts of Interest: The authors declare no conflict of interest.

References

1. Smith, A.H.; Lingas, E.O.; Rahman, M. Contamination of drinking-water by arsenic in Bangladesh: A public health emergency. *Bull. World Health Organ.* **2000**, *78*, 1093–1103. [PubMed]
2. Pearshouse, R. *Nepotism and Neglect: The Failing Response to Arsenic in the Drinking Water of Bangladesh's Rural Poor*; Human Rights Watch: New York, NY, USA, 2016; Available online: https://books.google.co.in/books?id=6kfljwEACAAJ (accessed on 12 March 2023).
3. Flanagan, S.V.; Johnston, R.B.; Zheng, Y. Arsenic in tube well water in Bangladesh: Health and economic impacts and implications for arsenic mitigation. *Bull. World Health Organ.* **2012**, *90*, 839–846. [CrossRef] [PubMed]
4. Smedley, P.L.; Kinniburgh, D.G. A review of the source, behaviour and distribution of arsenic in natural waters. *Appl. Geochem.* **2002**, *17*, 517–568. [CrossRef]
5. Mukherjee, A.; Verma, S.; Gupta, S.; Henke, K.R.; Bhattacharya, P. Influence of tectonics, sedimentation and aqueous flow cycles on the origin of global groundwater arsenic: Paradigms from three continents. *J. Hydrol.* **2014**, *518*, 284–299. [CrossRef]
6. Chakraborty, M.; Mukherjee, A.; Ahmed, K.M. A Review of Groundwater Arsenic in the Bengal Basin, Bangladesh and India: From Source to Sink. *Curr. Pollut. Rep.* **2015**, *1*, 220–247. [CrossRef]
7. Nickson, R.; McArthur, J.; Ravenscroft, P.; Burgess, W.; Ahmed, K. Mechanism of arsenic release to groundwater, Bangladesh and West Bengal. *Appl. Geochem.* **2000**, *15*, 403–413. [CrossRef]
8. Nickson, R.; McArthur, J.; Burgess, W.; Ahmed, K.M.; Ravenscroft, P.; Rahmanñ, M. Arsenic poisoning of Bangladesh groundwater. *Nature* **1998**, *395*, 338. [CrossRef]
9. Bhattacharya, P.; Jacks, G.; Jana, J.; Sracek, A.; Gustafsson, J.; Chatterjee, D. Geochemistry of the Holocene alluvial sediments of Bengal Delta Plain from West Bengal, India: Implications on arsenic contamination in groundwater. *Groundw. Arsen. Contam. Bengal Delta Plain Bangladesh* **2001**, *3084*, 21–40.
10. McArthur, J.; Ravenscroft, P.; Safiulla, S.; Thirlwall, M.F. Arsenic in groundwater: Testing pollution mechanisms for sedimentary aquifers in Bangladesh. *Water Resour. Res.* **2001**, *37*, 109–117. [CrossRef]
11. McArthur, J.; Banerjee, D.; Hudson-Edwards, K.; Mishra, R.; Purohit, R.; Ravenscroft, P.; Cronin, A.; Howarth, R.; Chatterjee, A.; Talukder, T. Natural organic matter in sedimentary basins and its relation to arsenic in anoxic ground water: The example of West Bengal and its worldwide implications. *Appl. Geochem.* **2004**, *19*, 1255–1293. [CrossRef]
12. Islam, F.S.; Gault, A.G.; Boothman, C.; Polya, D.A.; Charnock, J.M.; Chatterjee, D.; Lloyd, J.R. Role of metal-reducing bacteria in arsenic release from Bengal delta sediments. *Nature* **2004**, *430*, 68–71. [CrossRef] [PubMed]
13. Zheng, Y.; Stute, M.; van Geen, A.; Gavrieli, I.; Dhar, R.; Simpson, H.; Schlosser, P.; Ahmed, K. Redox control of arsenic mobilization in Bangladesh groundwater. *Appl. Geochem.* **2004**, *19*, 201–214. [CrossRef]
14. Hasan, M.A.; Ahmed, K.M.; Sracek, O.; Bhattacharya, P.; von Brömssen, M.; Broms, S.; Fogelström, J.; Mazumder, M.L.; Jacks, G. Arsenic in shallow groundwater of Bangladesh: Investigations from three different physiographic settings. *Hydrogeol. J.* **2007**, *15*, 1507–1522. [CrossRef]
15. Glodowska, M.; Stopelli, E.; Schneider, M.; Lightfoot, A.; Rathi, B.; Straub, D.; Patzner, M.; Duyen, V.; Members, A.T.; Berg, M. Role of in situ natural organic matter in mobilizing As during microbial reduction of FeIII-mineral-bearing aquifer sediments from Hanoi (Vietnam). *Environ. Sci. Technol.* **2020**, *54*, 4149–4159. [CrossRef]
16. Qiao, W.; Guo, H.; He, C.; Shi, Q.; Xiu, W.; Zhao, B. Molecular Evidence of Arsenic Mobility Linked to Biodegradable Organic Matter. *Environ. Sci. Technol.* **2020**, *54*, 7280–7290. [CrossRef]
17. Vega, M.A.; Kulkarni, H.V.; Johannesson, K.H.; Taylor, R.J.; Datta, S. Mobilization of co-occurring trace elements (CTEs) in arsenic contaminated aquifers in the Bengal basin. *Appl. Geochem.* **2020**, *122*, 104709. [CrossRef]
18. Anawar, H.M.; Akai, J.; Komaki, K.; Terao, H.; Yoshioka, T.; Ishizuka, T.; Safiullah, S.; Kato, K. Geochemical occurrence of arsenic in groundwater of Bangladesh: Sources and mobilization processes. *J. Geochem. Explor.* **2003**, *77*, 109–131. [CrossRef]
19. Seddique, A.A.; Masuda, H.; Mitamura, M.; Shinoda, K.; Yamanaka, T.; Itai, T.; Maruoka, T.; Uesugi, K.; Ahmed, K.M.; Biswas, D.K. Arsenic release from biotite into a Holocene groundwater aquifer in Bangladesh. *Appl. Geochem.* **2008**, *23*, 2236–2248. [CrossRef]
20. Masuda, H.; Shinoda, K.; Okudaira, T.; Takahashi, Y.; Noguchi, N. Chlorite—Source of arsenic groundwater pollution in the Holocene aquifer of Bangladesh. *Geochem. J.* **2012**, *46*, 381–391. [CrossRef]
21. Redman, A.D.; Macalady, D.L.; Ahmann, D. Natural Organic Matter Affects Arsenic Speciation and Sorption onto Hematite. *Environ. Sci. Technol.* **2002**, *36*, 2889–2896. [CrossRef] [PubMed]
22. Wang, S.; Mulligan, C.N. Natural attenuation processes for remediation of arsenic contaminated soils and groundwater. *J. Hazard. Mater.* **2006**, *138*, 459–470. [CrossRef] [PubMed]
23. Anawar, K.K.H.; Komaki, K.; Akai, J.; Takada, J.; Ishizuka, T.; Takahashi, T.; Yoshioka, T.; Kato, K.; Anawar, H. Diagenetic control on arsenic partitioning in sediments of the Meghna River delta, Bangladesh. *Environ. Geol.* **2002**, *41*, 816–825. [CrossRef]
24. Varner, T.S.; Kulkarni, H.V.; Nguyen, W.; Kwak, K.; Cardenas, M.B.; Knappett, P.S.; Ojeda, A.S.; Malina, N.; Bhuiyan, M.U.; Ahmed, K.M.; et al. Contribution of sedimentary organic matter to arsenic mobilization along a potential natural reactive barrier (NRB) near a river: The Meghna river, Bangladesh. *Chemosphere* **2022**, *308*, 136289. [CrossRef]
25. Saha, S.; Reza, A.H.M.S.; Roy, M.K. Arsenic geochemistry of the sediments of the shallow aquifer and its correlation with the groundwater, Rangpur, Bangladesh. *Appl. Water Sci.* **2021**, *11*, 1–11. [CrossRef]

26. Nath, B.; Chakraborty, S.; Burnol, A.; Stüben, D.; Chatterjee, D.; Charlet, L. Mobility of arsenic in the sub-surface environment: An integrated hydrogeochemical study and sorption model of the sandy aquifer materials. *J. Hydrol.* **2009**, *364*, 236–248. [CrossRef]
27. Deng, Y.; Dixon, J.B.; Schulze, D.G. Soil Organic Matter and Organic-Mineral Interactions. *Soil Mineral. Environ. Appl.* **2018**, *7*, 69–107. [CrossRef]
28. Liu, G.; Fernandez, A.; Cai, Y. Complexation of Arsenite with Humic Acid in the Presence of Ferric Iron. *Environ. Sci. Technol.* **2011**, *45*, 3210–3216. [CrossRef]
29. Xue, Q.; Ran, Y.; Tan, Y.; Peacock, C.L.; Du, H. Arsenite and arsenate binding to ferrihydrite organo-mineral coprecipitate: Implications for arsenic mobility and fate in natural environments. *Chemosphere* **2019**, *224*, 103–110. [CrossRef]
30. Goldberg, S. Competitive adsorption of arsenate and arsenite on oxides and clay minerals. *Soil Sci. Soc. Am. J.* **2002**, *66*, 413–421. [CrossRef]
31. Beaulieu, B.T.; Savage, K.S. Arsenate Adsorption Structures on Aluminum Oxide and Phyllosilicate Mineral Surfaces in Smelter-Impacted Soils. *Environ. Sci. Technol.* **2005**, *39*, 3571–3579. [CrossRef]
32. Charlet, L.; Chakraborty, S.; Appelo, C.; Roman-Ross, G.; Nath, B.; Ansari, A.; Lanson, M.; Chatterjee, D.; Mallik, S.B. Chemodynamics of an arsenic "hotspot" in a West Bengal aquifer: A field and reactive transport modeling study. *Appl. Geochem.* **2007**, *22*, 1273–1292. [CrossRef]
33. Tabelin, C.B.; Sasaki, R.; Igarashi, T.; Park, I.; Tamoto, S.; Arima, T.; Ito, M.; Hiroyoshi, N. Simultaneous leaching of arsenite, arsenate, selenite and selenate, and their migration in tunnel-excavated sedimentary rocks: II. Kinetic and reactive transport modeling. *Chemosphere* **2017**, *188*, 444–454. [CrossRef]
34. Huyen, D.T.; Tabelin, C.B.; Thuan, H.M.; Dang, D.H.; Truong, P.T.; Vongphuthone, B.; Kobayashi, M.; Igarashi, T. The solid-phase partitioning of arsenic in unconsolidated sediments of the Mekong Delta, Vietnam and its modes of release under various conditions. *Chemosphere* **2019**, *233*, 512–523. [CrossRef]
35. Hofstetter, T.B.; Schwarzenbach, R.P.; Haderlein, S.B. Reactivity of Fe(II) Species Associated with Clay Minerals. *Environ. Sci. Technol.* **2003**, *37*, 519–528. [CrossRef] [PubMed]
36. Neumann, A.; Hofstetter, T.B.; Lüssi, M.; Cirpka, O.A.; Petit, S.; Schwarzenbach, R.P. Assessing the Redox Reactivity of Structural Iron in Smectites Using Nitroaromatic Compounds As Kinetic Probes. *Environ. Sci. Technol.* **2008**, *42*, 8381–8387. [CrossRef] [PubMed]
37. Neumann, A.; Hofstetter, T.; Skarpeli-Liati, M.; Schwarzenbach, R.P. Reduction of Polychlorinated Ethanes and Carbon Tetrachloride by Structural Fe(II) in Smectites. *Environ. Sci. Technol.* **2009**, *43*, 4082–4089. [CrossRef]
38. Huang, J.; Jones, A.; Waite, T.D.; Chen, Y.; Huang, X.; Rosso, K.M.; Kappler, A.; Mansor, M.; Tratnyek, P.G.; Zhang, H. Fe(II) Redox Chemistry in the Environment. *Chem. Rev.* **2021**, *121*, 8161–8233. [CrossRef] [PubMed]
39. Guénet, H.; Davranche, M.; Vantelon, D.; Coz, M.B.-L.; Jardé, E.; Dorcet, V.; Demangeat, E.; Jestin, J. Highlighting the wide variability in arsenic speciation in wetlands: A new insight into the control of the behavior of arsenic. *Geochim. Cosmochim. Acta* **2017**, *203*, 284–302. [CrossRef]
40. Stucki, J. *Chapter 8 Properties and Behaviour of Iron in Clay Minerals*; Elsevier: Amsterdam, The Netherlands, 2006; Volume 1, pp. 423–475. [CrossRef]
41. Stucki, J.W. A review of the effects of iron redox cycles on smectite properties. *Comptes Rendus Geosci.* **2011**, *343*, 199–209. [CrossRef]
42. Zhang, W.; Li, X.; Shen, J.; Sun, Z.; Zhou, X.; Li, F.; Ma, F.; Gu, Q. Insights into the degradation process of phenol during in-situ thermal desorption: The overlooked oxidation of hydroxyl radicals from oxygenation of reduced Fe-bearing clay minerals. *J. Hazard. Mater.* **2023**, *444*, 130401. [CrossRef]
43. Farmer, V.C. *The Anhydrous Oxide Minerals*; Mineralogical Society of Great Britain and Ireland: London UK, 1974; pp. 183–204. [CrossRef]
44. Russell, J.; Fraser, A. Infrared methods. In *Clay Mineralogy: Spectroscopic and Chemical Determinative Methods*; Springer Science & Business Media: Berlin, Germany, 1994; pp. 11–67.
45. Frost, R.L.; Ruan, H.; Kloprogge, J.T.; Gates, W. Dehydration and dehydroxylation of nontronites and ferruginous smectite. *Thermochim. Acta* **2000**, *346*, 63–72. [CrossRef]
46. Frost, R.L.; Kloprogge, J.T.; Russell, S.C.; Szetu, J.L. Vibrational Spectroscopy and Dehydroxylation of Aluminum (Oxo)Hydroxides: Gibbsite. *Appl. Spectrosc.* **1999**, *53*, 423–434. [CrossRef]
47. Ruan, H.; Frost, R.; Kloprogge, J.; Duong, L. Infrared spectroscopy of goethite dehydroxylation: III. FT-IR microscopy of in situ study of the thermal transformation of goethite to hematite. *Spectrochim. Acta Part A Mol. Biomol. Spectrosc.* **2002**, *58*, 967–981. [CrossRef] [PubMed]
48. Parikh, S.J.; Goyne, K.W.; Margenot, A.J.; Mukome, F.N.; Calderón, F.J. Soil Chemical Insights Provided through Vibrational Spectroscopy. *Adv. Agron.* **2014**, *126*, 1–148. [CrossRef]
49. Madejová, J.; Gates, W.; Petit, S. IR spectra of clay minerals. In *Developments in Clay Science*; Elsevier: Amsterdam, The Netherlands, 2017; Volume 8, pp. 107–149.
50. Torrent, J.; Barrón, V. Diffuse reflectance spectroscopy of iron oxides. *Encycl. Surf. Colloid Sci.* **2002**, *1*, 1438–1446.
51. Edwards, H.; Drummond, L.; Russ, J. Fourier-transform Raman spectroscopic study of pigments in native American Indian rock art: Seminole Canyon. *Spectrochim. Acta Part A Mol. Biomol. Spectrosc.* **1998**, *54*, 1849–1856. [CrossRef]

52. Jordán, M.; Sanfeliu, T.; de la Fuente, C. Firing transformations of Tertiary clays used in the manufacturing of ceramic tile bodies. *Appl. Clay Sci.* **2001**, *20*, 87–95. [CrossRef]
53. de Faria, D.L.A.; Lopes, F.N. Heated goethite and natural hematite: Can Raman spectroscopy be used to differentiate them? *Vib. Spectrosc.* **2007**, *45*, 117–121. [CrossRef]
54. Manoharan, C.; Sutharsan, P.; Dhanapandian, S.; Venkatachalapathy, R.; Asanulla, R.M. Analysis of temperature effect on ceramic brick production from alluvial deposits, Tamilnadu, India. *Appl. Clay Sci.* **2011**, *54*, 20–25. [CrossRef]
55. Murad, E.; Wagner, U. Clays and clay minerals: The firing process. *Hyperfine Interact.* **1998**, *117*, 337–356. [CrossRef]
56. Murad, E.; Wagner, U. The thermal behaviour of an Fe-rich illite. *Clay Miner.* **1996**, *31*, 45–52. [CrossRef]
57. Mukherjee, A.; Fryar, A.E.; Thomas, W.A. Geologic, geomorphic and hydrologic framework and evolution of the Bengal basin, India and Bangladesh. *J. Asian Earth Sci.* **2009**, *34*, 227–244. [CrossRef]
58. Alam, M.; Alam, M.M.; Curry, J.R.; Chowdhury, M.L.R.; Gani, M.R. An overview of the sedimentary geology of the Bengal Basin in relation to the regional tectonic framework and basin-fill history. *Sediment. Geol.* **2003**, *155*, 179–208. [CrossRef]
59. Steckler, M.S.; Nooner, S.L.; Akhter, S.H.; Chowdhury, S.K.; Bettadpur, S.; Seeber, L.; Kogan, M.G. Modeling Earth deformation from monsoonal flooding in Bangladesh using hydrographic, GPS, and Gravity Recovery and Climate Experiment (GRACE) data. *J. Geophys. Res. Solid Earth* **2010**, *115*, B08407. [CrossRef]
60. Steckler, M.S.; Akhter, S.H.; Seeber, L. Collision of the Ganges–Brahmaputra Delta with the Burma Arc: Implications for earthquake hazard. *Earth Planet. Sci. Lett.* **2008**, *273*, 367–378. [CrossRef]
61. McArthur, J.M.; Ravenscroft, P.; Banerjee, D.M.; Milsom, J.; Hudson-Edwards, K.A.; Sengupta, S.; Bristow, C.S.; Sarkar, A.; Tonkin, S.; Purohit, R. How paleosols influence groundwater flow and arsenic pollution: A model from the Bengal Basin and its worldwide implication. *Water Resour. Res.* **2008**, *44*, W11411. [CrossRef]
62. Pickering, J.; Diamond, M.; Goodbred, S.; Grall, C.; Martin, J.; Palamenghi, L.; Paola, C.; Schwenk, T.; Sincavage, R.; Spiess, V. Impact of glacial-lake paleofloods on valley development since glacial termination II: A conundrum of hydrology and scale for the lowstand Brahmaputra-Jamuna paleovalley system. *GSA Bull.* **2019**, *131*, 58–70. [CrossRef]
63. Goodbred, S.L.; Kuehl, S.A.; Steckler, M.S.; Sarker, M.H. Controls on facies distribution and stratigraphic preservation in the Ganges–Brahmaputra delta sequence. *Sediment. Geol.* **2003**, *155*, 301–316. [CrossRef]
64. Pedrazas, M.N.; Cardenas, M.B.; Hosain, A.; Demir, C.; Ahmed, K.M.; Akhter, S.H.; Wang, L.; Datta, S.; Knappett, P.S.K. Application of electrical resistivity to map the stratigraphy and salinity of fluvio-deltaic aquifers: Case studies from Bangladesh that reveal benefits and pitfalls. *Hydrogeol. J.* **2021**, *29*, 1601–1610. [CrossRef]
65. Horneman, A.; van Geen, A.; Kent, D.; Mathe, P.; Zheng, Y.; Dhar, R.; O'connell, S.; Hoque, M.; Aziz, Z.; Shamsudduha, M.; et al. Decoupling of As and Fe release to Bangladesh groundwater under reducing conditions. Part I: Evidence from sediment profiles. *Geochim. Cosmochim. Acta* **2004**, *68*, 3459–3473. [CrossRef]
66. van Geen, A.; Ahmed, E.B.; Pitcher, L.; Mey, J.L.; Ahsan, H.; Graziano, J.H.; Ahmed, K.M. Comparison of two blanket surveys of arsenic in tubewells conducted 12 years apart in a 25 km^2 area of Bangladesh. *Sci. Total. Environ.* **2014**, *488–489*, 484–492. [CrossRef] [PubMed]
67. van Geen, A.; Zheng, Y.; Versteeg, R.; Stute, M.; Horneman, A.; Dhar, R.; Steckler, M.; Gelman, A.; Small, C.; Ahsan, H.; et al. Spatial variability of arsenic in 6000 tube wells in a 25 km^2 area of Bangladesh. *Water Resour. Res.* **2003**, *39*, 1140–1155. [CrossRef]
68. BGS&DPHE. *Arsenic Contamination of Groundwater in Bangladesh*; British Geological Survey Department of Public Health Engineering: London, UK, 2001; p. 630.
69. Datta, S.; Mailloux, B.; Jung, H.-B.; Hoque, M.A.; Stute, M.; Ahmed, K.M.; Zheng, Y. Redox trapping of arsenic during groundwater discharge in sediments from the Meghna riverbank in Bangladesh. *Proc. Natl. Acad. Sci. USA* **2009**, *106*, 16930–16935. [CrossRef]
70. Jung, H.B.; Zheng, Y.; Rahman, M.W.; Ahmed, K.M. Redox zonation and oscillation in the hyporheic zone of the Ganges-Brahmaputra-Meghna Delta: Implications for the fate of groundwater arsenic during discharge. *Appl. Geochem.* **2015**, *63*, 647–660. [CrossRef] [PubMed]
71. Jung, H.B.; Bostick, B.C.; Zheng, Y. Field, Experimental, and Modeling Study of Arsenic Partitioning across a Redox Transition in a Bangladesh Aquifer. *Environ. Sci. Technol.* **2011**, *46*, 1388–1395. [CrossRef] [PubMed]
72. Shuai, P.; Knappett, P.S.K.; Hossain, S.; Hosain, A.; Rhodes, K.; Ahmed, K.M.; Cardenas, M.B. The Impact of the Degree of Aquifer Confinement and Anisotropy on Tidal Pulse Propagation. *Groundwater* **2017**, *55*, 519–531. [CrossRef] [PubMed]
73. Berube, M.; Jewell, K.; Myers, K.D.; Knappett, P.S.K.; Shuai, P.; Hossain, A.; Lipsi, M.; Hossain, S.; Hossain, A.; Aitkenhead-Peterson, J.; et al. The fate of arsenic in groundwater discharged to the Meghna River, Bangladesh. *Environ. Chem.* **2018**, *15*, 29. [CrossRef]
74. Strens, R.G.J.; Wood, B.J. Diffuse reflectance spectra and optical properties of some iron and titanium oxides and oxyhydroxides. *Miner. Mag.* **1979**, *43*, 347–354. [CrossRef]
75. Morris, R.V.; Lauer, H.V., Jr.; Lawson, C.A.; Gibson, E.K., Jr.; Nace, G.A.; Stewart, C. Spectral and other physicochemical properties of submicron powders of hematite (α-Fe_2O_3), maghemite (γ-Fe_2O_3), magnetite (Fe_3O_4), goethite (α-FeOOH), and lepidocrocite (γ-FeOOH). *J. Geophys. Res. Solid Earth* **1985**, *90*, 3126–3144. [CrossRef]
76. USEPA. *Method 6200, Revision 0, February 2007: Field Portable X-ray Fluorescence Spectrometry for the Determination of Elemental Concentrations in Soil and Sediment*; EPA Publication SW-846: Washington, DC, USA, 2007. Available online: https://www.epa.gov/sites/default/files/2015-12/documents/6200.pdf (accessed on 3 March 2023).
77. Farmer, V. The Layer Silicates. In *the Infrared Spectra of Minerals*; Mineralogical Society: London, UK, 1974; pp. 331–363.

78. Chen, S.A.; Heaney, P.J.; Post, J.E.; Fischer, T.B.; Eng, P.J.; Stubbs, J.E. Superhydrous hematite and goethite: A potential water reservoir in the red dust of Mars? *Geology* **2021**, *49*, 1343–1347. [CrossRef]
79. Prasad, P.; Prasad, K.S.; Chaitanya, V.K.; Babu, E.; Sreedhar, B.; Murthy, S.R. In situ FTIR study on the dehydration of natural goethite. *J. Asian Earth Sci.* **2006**, *27*, 503–511. [CrossRef]
80. Margenot, A.J.; Calderón, F.J.; Goyne, K.W.; Dmukome, F.N.; Parikh, S. IR spectroscopy, soil analysis applications. In *Encyclopedia of Spectroscopy and Spectrometry*; Elsevier: Amsterdam, The Netherlands, 2016; pp. 448–454.
81. Lugassi, R.; Ben-Dor, E.; Eshel, G. Reflectance spectroscopy of soils post-heating—Assessing thermal alterations in soil minerals. *Geoderma* **2014**, *213*, 268–279. [CrossRef]
82. Balsam, W.L.; Damuth, J.E. Further investigations of shipboard vs. shore-based spectral data: Implications for interpreting leg 164 sediment composition1. *Proc. Ocean Drill. Program Sci. Results* **2000**, *164*, 313–324.
83. Arimoto, R.; Balsam, W.; Schloesslin, C. Visible spectroscopy of aerosol particles collected on filters: Iron-oxide minerals. *Atmos. Environ.* **2002**, *36*, 89–96. [CrossRef]
84. Wu, G.; Xu, T.; Zhang, X.; Zhang, C.; Yan, N. The visible spectroscopy of iron oxide minerals in dust particles from ice cores on the Tibetan Plateau. *Tellus B Chem. Phys. Meteorol.* **2016**, *68*, 29191. [CrossRef]
85. Cao, W.; Jiang, Z.; Gai, C.; Barrón, V.; Torrent, J.; Zhong, Y.; Liu, Q. Re-Visiting the Quantification of Hematite by Diffuse Reflectance Spectroscopy. *Minerals* **2022**, *12*, 872. [CrossRef]
86. Kadir, S.; Erman, H.; Erkoyun, H. Mineralogical and geochemical characteristics and genesis of hydrothermal kaolinite deposits within Neogene volcanites, Kütahya (western Anatolia), Turkey. *Clays Clay Miner.* **2011**, *59*, 250–276. [CrossRef]
87. Komadel, P.; Madejová, J.; Stucki, J.W. Structural Fe (III) reduction in smectites. *Appl. Clay Sci.* **2006**, *34*, 88–94. [CrossRef]
88. Gasparini, E.; Tarantino, S.C.; Ghigna, P.; Riccardi, M.P.; Cedillo-González, E.I.; Siligardi, C.; Zema, M. Thermal dehydroxylation of kaolinite under isothermal conditions. *Appl. Clay Sci.* **2013**, *80–81*, 417–425. [CrossRef]
89. Smykatz-Kloss, W.; Heide, K.; Klinke, W. Applications of thermal methods in the geosciences. In *Handbook of Thermal Analysis and Calorimetry*; Elsevier: Amsterdam, The Netherlands, 2003; Volume 2, pp. 451–593.
90. Gaines, G.L.; Vedder, W. Dehydroxylation of Muscovite. *Nature* **1964**, *201*, 495. [CrossRef]
91. Nesbitt, H.W.; Young, G.M. Early Proterozoic climates and plate motions inferred from major element chemistry of lutites. *Nature* **1982**, *299*, 715–717. [CrossRef]
92. Gazi, M.Y.; Apu, S.I.; Sharmili, N.; Rahman, M.Z. Origin and characterization of clay deposits in the Dupi Tila Formation of the Bengal Basin, Bangladesh. *Solid Earth Sci.* **2021**, *6*, 313–327. [CrossRef]
93. Fedo, C.M.; Wayne Nesbitt, H.; Young, G.M. Unraveling the effects of potassium metasomatism in sedimentary rocks and paleosols, with implications for paleoweathering conditions and provenance. *Geology* **1995**, *23*, 921–924. [CrossRef]
94. Allison, M.A.; Khan, S.; Goodbred, S.L., Jr.; Kuehl, S.A. Stratigraphic evolution of the late Holocene Ganges–Brahmaputra lower delta plain. *Sediment. Geol.* **2003**, *155*, 317–342. [CrossRef]
95. Khan, H.R.; Liu, J.; Liu, S.; Seddique, A.A.; Cao, L.; Rahman, A. Clay mineral compositions in surface sediments of the Ganges-Brahmaputra-Meghna river system of Bengal Basin, Bangladesh. *Mar. Geol.* **2019**, *412*, 27–36. [CrossRef]
96. Ayers, J.C.; Patton, B.; Dietrich, M. Preliminary Evidence of Transport-Limited Chemical Weathering and Element Immobility in the Ganges Tidal Delta Plain of Bangladesh. *Geochem. Geophys. Geosystems* **2020**, *21*, e2020GC009029. [CrossRef]
97. Dewan, A.; Mustafi, S.; Ahsan, M.; Ullah, M.S. Investigation on physical properties of patia clay (Chittagong), Bangladesh. *Bangladesh J. Sci. Ind. Res.* **2014**, *49*, 255–262. [CrossRef]
98. Chakraborty, S.; Wolthers, M.; Chatterjee, D.; Charlet, L. Adsorption of arsenite and arsenate onto muscovite and biotite mica. *J. Colloid Interface Sci.* **2007**, *309*, 392–401. [CrossRef]
99. Pedersen, H.D.; Postma, D.; Jakobsen, R. Release of arsenic associated with the reduction and transformation of iron oxides. *Geochim. Et Cosmochim. Acta* **2006**, *70*, 4116–4129. [CrossRef]
100. Shi, Z.; Hu, S.; Lin, J.; Liu, T.; Li, X.; Li, F. Quantifying Microbially Mediated Kinetics of Ferrihydrite Transformation and Arsenic Reduction: Role of the Arsenate-Reducing Gene Expression Pattern. *Environ. Sci. Technol.* **2020**, *54*, 6621–6631. [CrossRef]
101. Wenzel, W.W.; Kirchbaumer, N.; Prohaska, T.; Stingeder, G.; Lombi, E.; Adriano, D.C. Arsenic fractionation in soils using an improved sequential extraction procedure. *Anal. Chim. Acta* **2001**, *436*, 309–323. [CrossRef]
102. Sun, J.; Mailloux, B.J.; Chillrud, S.N.; van Geen, A.; Thompson, A.; Bostick, B.C. Simultaneously quantifying ferrihydrite and goethite in natural sediments using the method of standard additions with X-ray absorption spectroscopy. *Chem. Geol.* **2018**, *476*, 248–259. [CrossRef] [PubMed]
103. Pomiès, M.P.; Menu, M.; Vignaud, C. Red palaeolithic pigments: Natural hematite or heated goethite? *Archaeometry* **1999**, *41*, 275–285. [CrossRef]
104. Liu, H.; Chen, T.; Zou, X.; Qing, C.; Frost, R.L. Thermal treatment of natural goethite: Thermal transformation and physical properties. *Thermochim. Acta* **2013**, *568*, 115–121. [CrossRef]
105. Murad, E.; Wagner, U.; Wagner, F.; Häusler, W. The thermal reactions of montmorillonite: A Mössbauer study. *Clay Miner.* **2002**, *37*, 583–590. [CrossRef]
106. Araújo, J.H.D.; Silva, N.F.D.; Acchar, W.; Gomes, U.U. Thermal decomposition of illite. *Mater. Res.* **2004**, *7*, 359–361. [CrossRef]
107. Ruan, H.; Frost, R.; Kloprogge, J. The behavior of hydroxyl units of synthetic goethite and its dehydroxylated product hematite. *Spectrochim. Acta Part A Mol. Biomol. Spectrosc.* **2001**, *57*, 2575–2586. [CrossRef]

108. Liu, H.; Chen, T.; Qing, C.; Xie, Q.; Frost, R.L. Confirmation of the assignment of vibrations of goethite: An ATR and IES study of goethite structure. *Spectrochim. Acta Part A Mol. Biomol. Spectrosc.* **2013**, *116*, 154–159. [CrossRef]
109. Walter, D.; Buxbaum, G.; Laqua, W. The Mechanism of the Thermal Transformation from Goethite to Hematite. *J. Therm. Anal. Calorim.* **2001**, *63*, 733–748. [CrossRef]
110. Wang, J.; Tomita, A. A Chemistry on the Volatility of Some Trace Elements during Coal Combustion and Pyrolysis. *Energy Fuels* **2003**, *17*, 954–960. [CrossRef]
111. Senior, C.L.; Bool, L.E., III; Morency, J.R. Laboratory study of trace element vaporization from combustion of pulverized coal. *Fuel Process. Technol.* **2000**, *63*, 109–124. [CrossRef]
112. Guo, R.; Yang, J.; Liu, Z. Thermal and chemical stabilities of arsenic in three Chinese coals. *Fuel Process. Technol.* **2004**, *85*, 903–912. [CrossRef]
113. Cheng, R.; Zhang, H.; Ni, H. Arsenic Removal from Arsenopyrite-Bearing Iron Ore and Arsenic Recovery from Dust Ash by Roasting Method. *Processes* **2019**, *7*, 754. [CrossRef]
114. Liu, H.; Pan, W.-P.; Wang, C.; Zhang, Y. Volatilization of Arsenic During Coal Combustion Based on Isothermal Thermogravimetric Analysis at 600–1500 °C. *Energy Fuels* **2016**, *30*, 6790–6798. [CrossRef]
115. Wang, C.; Liu, H.; Zhang, Y.; Zou, C.; Anthony, E.J. Review of arsenic behavior during coal combustion: Volatilization, transformation, emission and removal technologies. *Prog. Energy Combust. Sci.* **2018**, *68*, 1–28. [CrossRef]
116. Gray, D.B.; Watts, F.; Overcamp, T.J. Volatility of Arsenic in Contaminated Clay at High Temperatures. *Environ. Eng. Sci.* **2001**, *18*, 1–7. [CrossRef]
117. Liu, W.; Xie, X.; Wang, Y. Novel insight into arsenic enrichment in aquifer sediments under different paleotemperatures from a molecular-level characterization of sedimentary organic matter. *J. Hazard. Mater.* **2023**, *451*, 131115. [CrossRef]
118. Jiang, J.-Q.; Ashekuzzaman, S.M.; Jiang, A.; Sharifuzzaman, S.M.; Chowdhury, S.R. Arsenic Contaminated Groundwater and Its Treatment Options in Bangladesh. *Int. J. Environ. Res. Public Health* **2013**, *10*, 18–46. [CrossRef]
119. Doušová, B.; Lhotka, M.; Grygar, T.; Machovič, V.; Herzogová, L. In situ co-adsorption of arsenic and iron/manganese ions on raw clays. *Appl. Clay Sci.* **2011**, *54*, 166–171. [CrossRef]
120. Acharyya, S.K.; Lahiri, S.; Raymahshay, B.C.; Bhowmik, A. Arsenic toxicity of groundwater in parts of the Bengal basin in India and Bangladesh: The role of Quaternary stratigraphy and Holocene sea-level fluctuation. *Environ. Geol.* **2000**, *39*, 1127–1137. [CrossRef]